High-throughput imaging of neuronal activity in *Caenorhabditis elegans*

Johannes Larsch[a,b], Donovan Ventimiglia[a,b], Cornelia I. Bargmann[a,b,1], and Dirk R. Albrecht[a,b,c,1]

[a]Howard Hughes Medical Institute and [b]Lulu and Anthony Wang Laboratory of Neural Circuits and Behavior, The Rockefeller University, New York, NY 10065; and [c]Department of Biomedical Engineering, Worcester Polytechnic Institute, Worcester, MA 01609

Neuronal responses to sensory inputs can vary based on genotype, development, experience, or stochastic factors. Existing neuronal recording techniques examine a single animal at a time, limiting understanding of the variability and range of potential responses. To scale up neuronal recordings, we here describe a system for simultaneous wide-field imaging of neuronal calcium activity from at least 20 *Caenorhabditis elegans* animals under precise microfluidic chemical stimulation. This increased experimental throughput was used to perform a systematic characterization of chemosensory neuron responses to multiple odors, odor concentrations, and temporal patterns, as well as responses to pharmacological manipulation. The system allowed recordings from sensory neurons and interneurons in freely moving animals, whose neuronal responses could be correlated with behavior. Wide-field imaging provides a tool for comprehensive circuit analysis with elevated throughput in *C. elegans*.

Modern neuronal recording techniques are labor- and equipment-intensive, and generally designed to obtain maximal information from individual animals. However, individuals differ from one another. To understand the full range and variability of neuronal responses, it is desirable to apply high-throughput methods and systematic data collection to many animals under controlled stimulation conditions.

The nematode *Caenorhabditis elegans* is particularly amenable to high-throughput studies of neural and behavioral activity, which are facilitated by its small size, compact nervous system, ease of genetic modification, well-defined behavioral repertoire, and transparent body with optical access to single defined neurons. Optical neural recordings in *C. elegans* have primarily used high-magnification imaging of neurons expressing a genetically encoded calcium indicator such as GCaMP or cameleon. Glued preparations (1) or partial-body traps (2–4) enable imaging of calcium dynamics in head neurons, but immobilization limits the animal's behavioral repertoire. More complex behaviors can be visualized in freely moving animals on agar surfaces by using a moving stage or objective and computer-controlled feedback to track a moving animal and keep a specific neuron in view (5–8). These methods monitor a single animal at a time, as do optical and electrophysiological recording methods in flies, fish, and rodents, which rely upon complex surgeries, implanted sensors, and dedicated equipment for each animal (9–13).

Here we describe a strategy for recording neuronal activity evoked by precise chemical stimulation of freely moving or anesthetized *C. elegans* by using wide-field microscopy. We adapted previous microfluidic arenas optimized for normal *C. elegans* crawling behavior and repeatable spatiotemporal stimulation (14) to simultaneous optical recording of calcium transients in individual neurons. The automated microscope is capable of continuous recording from more than 20 animals at once for hours during repeated stimulation without user interaction. We demonstrate the performance of this method by systematically surveying neural responses to stimulation parameters, testing pharmacological modulators of neural dynamics, and correlating stimulus-evoked locomotory behaviors with calcium dynamics in several chemosensory neurons and interneurons. Our results demonstrate broad capabilities of wide-field microscopy for neural imaging.

Results

Fluorescence Imaging at Low Magnification. Wide-field microscopy eases the challenge of neuron registration and focus in moving samples including live animals. As objective magnification (M) is reduced, the total volume from which light is projected onto the camera expands greatly, with the area field-of-view scaling by $1/M^2$ and axial depth-of-field by $\sim 1/M$. Fluorescent signals can be recorded from any neuron within this volume without stage tracking or focusing, as long as individual neurons can be resolved, motion blur is minimized, and signals exceed background noise. We met these requirements for calcium imaging of *C. elegans* neurons on a standard inverted epifluorescence microscope using high-N.A. objectives (2.5×/0.12 N.A. or 5×/0.25 N.A.) and a sensitive low-noise electron-multiplying (EM) CCD camera to maximize the signal-to-noise of fluorescence recordings, and fast-switching solid-state illumination to minimize motion artifacts and phototoxicity (Fig. 1A).

A microfluidic arena for *C. elegans* behavioral analysis (14) was miniaturized to keep animals within the 3.28×3.28 mm^2 field of view and ~ 50 μm depth of field at 2.5× magnification while delivering precise patterns of chemical stimulation. The fluidic design contained a structured micropost array for unimpeded crawling locomotion, barriers to prevent animal escape, and inlet channels tailored to present temporal pulses, spatial stripes, or linear gradients of liquid-borne stimuli (14) (Fig. 1B and Fig. S1). The microscope automatically controlled chemical

Significance

Most behaviors and neuronal responses are variable across individual animals and repeated presentation of the same stimulus. Current neuronal recording techniques examine one animal at a time, whereas hundreds to thousands of trials may be necessary to understand the probability and range of responses. We developed an imaging system to record neuronal activity, detected by genetically encoded calcium indicators, simultaneously from 20 *Caenorhabditis elegans* animals in microfluidic arenas. We used this system to characterize chemosensory neuron responses to odors and pharmacological manipulation. The system allowed recordings in freely moving animals, whose neuronal responses could be correlated with behavior. We found that behavioral variability is observed even when sensory responses are reproducible, and that sensitivity to specific odors varies among individual animals.
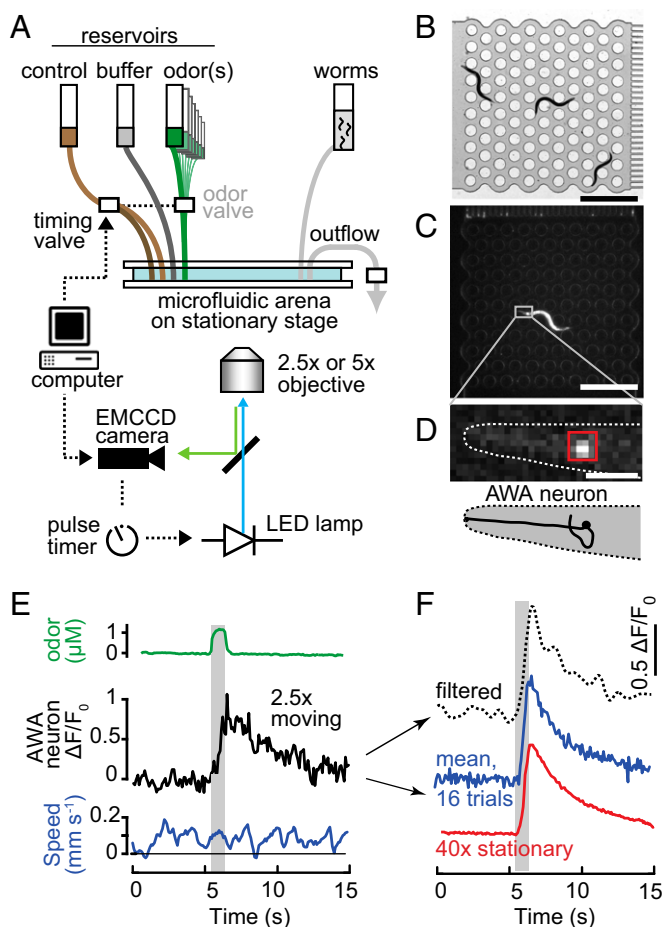
Fig. 1. Wide-field imaging of neural activity with precise microfluidic chemical stimulation. (*A*) Schematic of the automated microscope. Video acquisition and fluidic valves for chemical stimulation are computer-controlled; fluorescence illumination is pulsed via digital signals synchronized with each camera frame. No motorized stage or focus mechanisms are needed with low-magnification objectives and glass-mounted microfluidic arenas. (*B*) Bright-field image of the microfluidic arena containing three animals and dye to distinguish fluidic channels (gray) from microposts. (Scale bar, 1 mm.) (*C*) Full-frame camera image showing one adult animal expressing GCaMP2.2b in the AWA sensory neurons. (Scale bar, 1 mm.) (*D*) Magnified view of the head from *C*. Red box indicates the integration window. (Scale bar, 50 μm.) (*E*) AWA sensory neuron response (relative fluorescence, $\Delta F/F_0$) and speed of a moving animal responding to a 1-s pulse of 1 μM diacetyl odor (DA). (*F*) Comparison of the single fluorescence trace at 2.5× from *E*, filtered to quantify individual response magnitude and dynamics, the mean of 16 repeated stimulations of the same moving animal, and a single recording in a stationary animal at 40× magnification.

stimulation via fluidic valves, selecting the concentration and timing parameters according to a programmed pattern (Fig. 1*A*). A software suite, called NeuroTracker, tracked multiple animals as they traversed the arena, integrated fluorescent signals, corrected for background and illumination, and automatically detected behavioral responses, as described in *SI Note*.

The duration of optical neural recordings is typically limited by phototoxicity and photobleaching that reduce signal fidelity over time. Phototoxic damage in *C. elegans* is evident after 20 min of cumulative blue-light illumination by increased autofluorescence in many tissues (15, 16). In contrast, pulsed illumination (10 ms per 100-ms frame) did not cause photodamage over at least 2 h (Fig. S2). Short illumination pulses also prevented motion blur in animals moving as much as 2 mm·s^{-1}, 10-fold greater than mean crawling speed (Fig. S3 and Movie S1).

We expressed the genetically encoded calcium sensor GCaMP2.2b in the two AWA sensory neurons, which respond to the attractive odor diacetyl with an increase in intracellular calcium indicative of depolarization (17, 18). At 2.5× magnification, AWA neuron morphology could not be resolved as a result of spatial undersampling (6.4 μm per pixel, compared with an AWA cell body diameter of 3–5 μm), so a larger region of interest of standard size was used for analysis (Fig. 1 *C* and *D* and Fig. S4). In response to a 1-s pulse of diacetyl (10^{-7} dilution; 1.15 μM), we detected a rapid increase and then a gradual decline in the integrated fluorescence signal (Fig. 1*E*) that closely resembled standard high-magnification recordings of AWA GCaMP responses (Fig. 1*F*). The fluorescence signal-to-noise ratio was proportional to objective magnification but remained greater than ~10 at 2.5× (Fig. 1*F* and Fig. S5), a value sufficient for quantification of response magnitude and dynamics from temporally filtered single traces or averaged repeated trials. Thus, wide-field imaging at reduced resolution permits accurate measurement of GCaMP signal dynamics in individual *C. elegans* neurons.

High-Throughput Neural Recordings in Response to Dynamic Odor Stimuli. A unique aspect of the wide-field imaging system is the ability to monitor at least 20 animals at once (Fig. 2*A* and Movie S2), in contrast to high-magnification systems that focus closely on a single animal. Because maintaining the identity of so many moving animals is challenging, we first established that odor-evoked calcium transients in AWA sensory neurons were similar in the presence or absence of the paralytic acetylcholine agonist tetramisole (19) (Fig. 2*B*). Next, we measured 2,852 AWA calcium responses from a total of 40 immobilized animals subjected to repeated diacetyl pulses of varying concentration, duration, or rate of concentration change (dC/dt; Fig. 2).

All animals responded to diacetyl odor with increased fluorescence of the GCaMP2.2b indicator in AWA neurons (Fig. 2*C*). Habituation was evident during the first few odor presentations, resulting in a ~20% reduction in peak magnitude over five trials (Fig. 2 *C* and *D*). The peak and the initial slope of the AWA calcium response showed a dose-dependent increase across a 10^5-fold diacetyl concentration range from 1 nM to 100 μM (Fig. 2 *E* and *H*). The calcium response increased throughout the 10-s odor pulse for low and high odor concentrations, but decreased before odor was removed at intermediate concentrations (0.1–1 μM); this short-term desensitization recovered in the 50 s before the subsequent odor pulse. Peak AWA calcium levels increased with odor duration up to the saturation point (2 s at 1 μM; Fig. 2 *F* and *I*). The dC/dt affected the magnitude, slope, and apparent latency of the neural response (Fig. 2 *G* and *J*). Thus, AWA sensory neuron dynamics reflect the magnitude and the temporal properties of chemical stimuli.

A single animal's response was reliable with respect to each stimulation parameter, but differences were observed across individual animals. Dose–response curves for individual animals yielded EC_{50} values that varied by two orders of magnitude (Fig. S6). Response magnitude was more variable between animals than between repeated stimulation of one animal, and more variable for the first five trials than later repeats; hence, the most consistent calcium responses were obtained from an individual animal after a few preconditioning pulses (Fig. 2*D*).

Efficient Determination of a Neuron's Chemical Receptive Field. In previous studies, laborious behavioral assays and laser ablation experiments demonstrated that each *C. elegans* chemosensory neuron detects multiple odors, tastes, or pheromone stimuli (20). To more efficiently map chemical stimuli to sensory neurons, we used the wide-field imaging system to test AWA neural responses to 30 small-molecule odors (Fig. 3 *A* and *B*). Odors were delivered sequentially in triplicate from 96-well plates by using ~60 μL sample per trial.
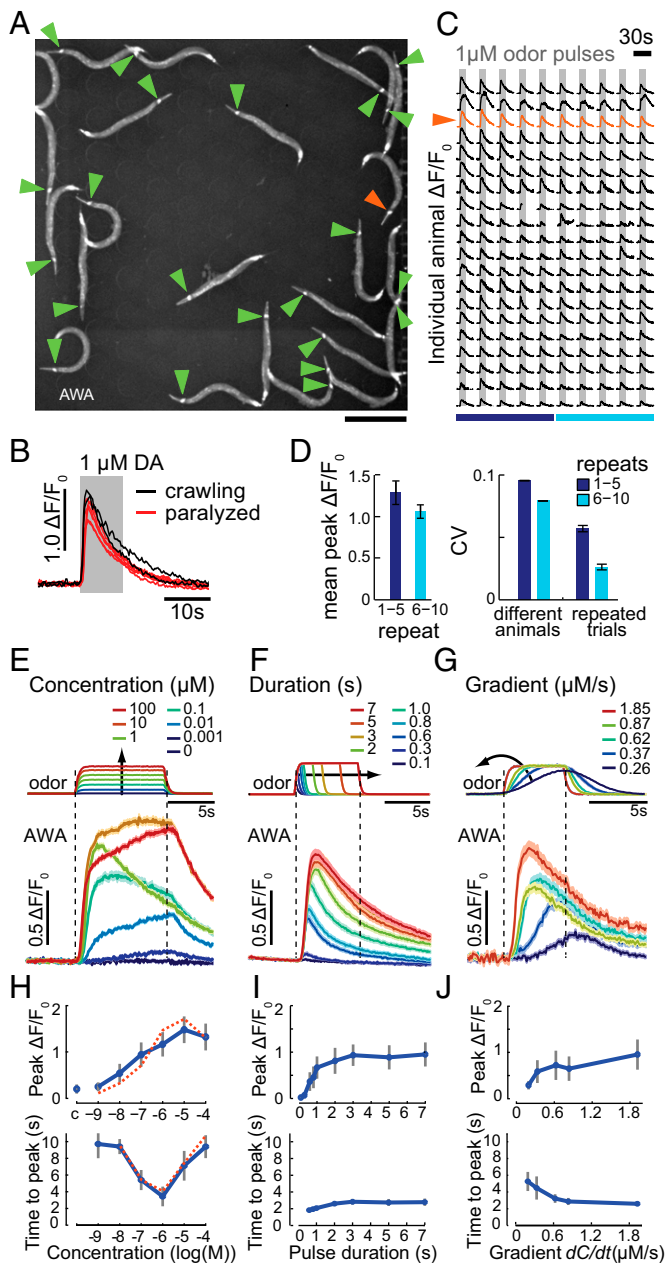
Fig. 2. High-throughput recording of neuronal responses. (*A*) Camera frame showing 23 animals expressing G-CaMP2.2b in AWA neurons (arrowheads). (Scale bar, 500 μm.) (*B*) AWA sensory neuron responses are similar in freely moving and paralyzed animals. Each curve represents mean fluorescence of one animal, *n* = 20 trials each for two moving and six paralyzed animals. (*C*) Odor-evoked fluorescence during 10 repeated 10-s pulses of 1 μM diacetyl at one pulse per minute. Each row represents an individual animal in *A*; orange trace is from the animal indicated by an orange arrowhead. (*D*) Mean peak AWA fluorescence and peak coefficient of variation (CV) for repeats 1 to 5 (dark blue) and 6 to 10 (light blue) calculated from data in *C*. (*E–G*) Mean AWA fluorescence response to systematic variation in (*E*) odor concentration (10-s pulses), (*F*) odor duration (1 μM diacetyl), (*G*) odor gradient (*dC/dt*; 5-s pulses, 0–1 μM diacetyl). Schematic (*Upper*) represents time course of stimulus modulation, measured from fluorescein dye controls. Light shading on calcium traces depicts SEM. (*H–J*) Mean (blue) AWA peak fluorescence and time of response peak are influenced by odor concentration (*H*), pulse duration (*I*), and odor gradient (*J*), as calculated from traces in *E–G*. The peak response appeared saturated at 10 μM diacetyl (10-s pulse, *E* and *H*), and at 3 s of stimulation (1 μM diacetyl, *F* and *I*). "C" represents control (buffer) stimulus. Orange curves represent the individual animal highlighted in *A* and *C*. For all data in *D–J*, error bars represent SD; *n* = 8–22 animals, one experiment per stimulus parameter, six to 12 trials per condition.

The known AWA-sensed odors diacetyl, pyrazine, 2,4,5-trimethylthiazole, and 2-methylpyrazine elicited robust calcium transients in nearly all tested animals (Fig. 3 *A* and *B*). Dose–response curves revealed a substantial variation across these four odors in sensitivity (Fig. 3*A*). A broad survey of odors tested at 10^{-6} dilution showed that benzaldehyde and butanone, known to be detected primarily by AWC neurons, did not elicit reliable responses in AWA (Fig. 3*B*).

Among previously uncharacterized odors, hexyl acetate elicited a response comparable to known AWA odors. Interestingly, several other acetates and alcohols elicited responses in only a subset of animals (Fig. 3*B*). These responses were consistently weak or strong across repeated stimulation of an individual, but uncorrelated to the strength of the individual's diacetyl response (Fig. 3 *D* and *E* and Fig. S7).

Similar experiments in *odr-10*(*ky32*) (*odor response abnormal*) mutant animals, which have a loss-of-function mutation in the diacetyl receptor (21), demonstrated greatly diminished AWA responses to 1 μM diacetyl, whereas responses for most other odors were preserved (Fig. 3 *B* and *C*). Mutant animals also failed to respond to the related odor 2,3-pentanedione, suggesting that ODR-10 contributes to its detection.

Pharmacological Modulation of Neural Activity. High-throughput pharmacological screening of *C. elegans* can identify new modulators of conserved biological pathways as well as antihelminthic agents (22–24). One such screen and subsequent genetic analysis identified nemadipine-A as a compound that induces morphological and egg-laying defects by antagonizing the α1-subunit of *C. elegans* L-type voltage gated calcium channels, EGL-19 (23). Reduced-function mutations in *egl-19* (*egg-laying defective*) and other L-type calcium channel blockers decrease stimulus-evoked calcium transients in ALM (25), ASH (26), and URX (27) sensory neurons, implicating the L-type channel in sensory activity. We assessed the suitability of the high-throughput system for chemical screening by examining the effects of nemadipine-A on AWA calcium transients. Animals were challenged with nine diacetyl pulses to establish a baseline response, then switched to 10 μM nemadipine-A for the next 10 diacetyl pulses, then returned to initial conditions (Fig. 4*A*). Within 1 min in nemadipine-A, the AWA calcium response was suppressed by ∼70%; this suppression recovered in 1 to 2 min after washout (Fig. 4*B*).

A dose–response curve for nemadipine-A inhibition of AWA calcium transients yielded an IC_{50} of 4.6 μM nemadipine-A (Fig. 4*C*), comparable to its 1 to 5 μM IC_{50} for egg-laying and morphological phenotypes (23). Nemadipine-A strongly inhibited AWA responses to low diacetyl concentrations, but had minimal effects at saturating diacetyl levels (Fig. 4*D*), suggesting that the voltage-gated EGL-19 channel amplifies AWA calcium signals to weak odor stimuli.

Neural Activity During Free-Moving Behavioral Responses. Direct observation of neuronal activity in unrestrained animals is essential for understanding how neural signals guide behavior. One interesting aspect of behavior is its variability in apparently constant conditions. For example, when *C. elegans* experiences removal of the attractive odor isoamyl alcohol (IAA), which is sensed by AWC sensory neurons, it can generate a pirouette (a reversal coupled to a sharp Ω-turn) or just a reversal, or it can fail to respond at all (14, 28). To characterize the neural signals associated with these responses, we subjected freely moving animals to 60 repeated IAA pulses and simultaneously recorded behavior and calcium transients in one AWC neuron that expressed the GCaMP3 calcium sensor (Fig. 5 *A–C* and Movie S3). Regardless of the behavioral outcome, the animal's AWC calcium transients had similar response dynamics and magnitude (Fig. 5 *C–E*). These observations suggest that AWC calcium transients reliably report sensory input and that the variable
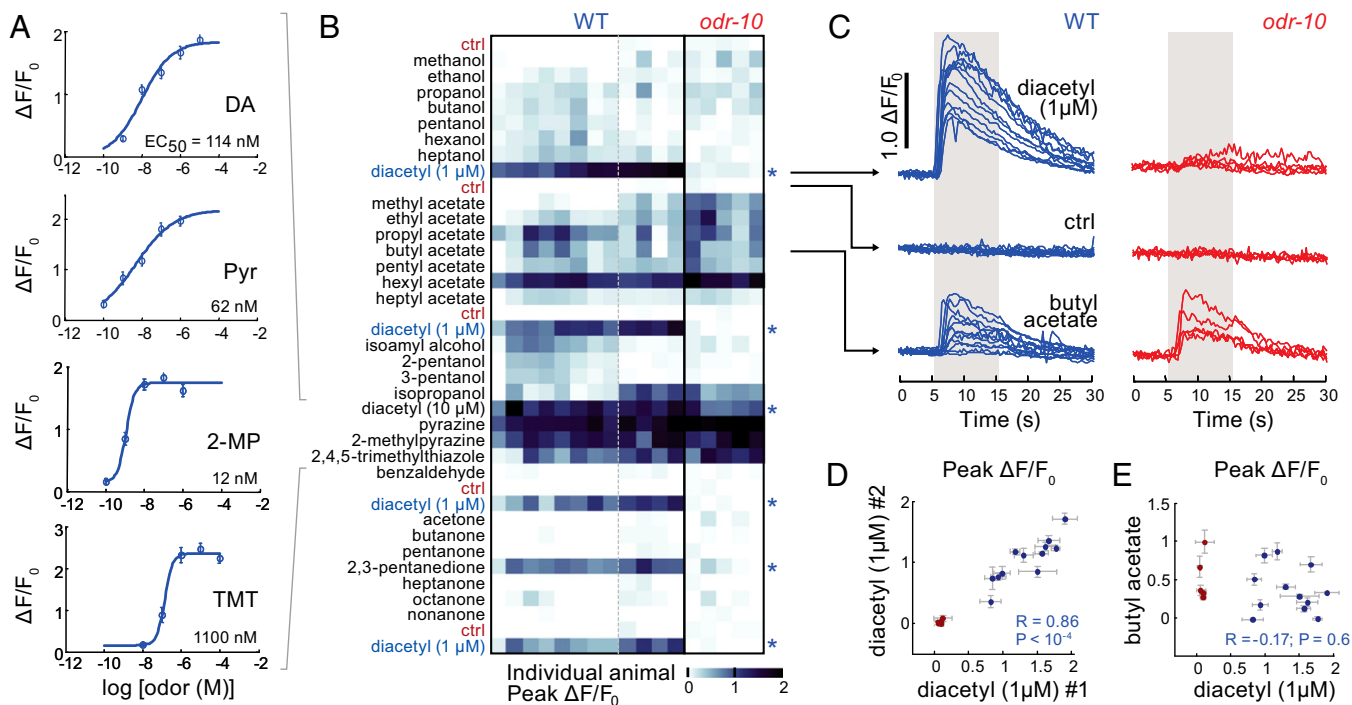

Fig. 3. Chemical screening of neuronal responses. (A) Neurometric curves of peak fluorescence in AWA neurons subjected to increasing concentrations of four odors. DA, diacetyl; Pyr, pyrazine; 2-MP, 2-methylpyrazine; TMT, 2,4,5-trimethylthiazole. Data are mean ± SEM; $n = 22$ traces (1 experiment, $n = 11$ animals, 2 trials each). (B) Small-molecule odor screen for AWA-detected odors. Thirty odors (10^{-6} dilution) were presented from a 96-well plate, sequentially and in triplicate, to 12 WT and 5 odr-10 mutant animals. Heat map shows mean peak fluorescence following odor addition. Multiple positive controls (1 μM diacetyl) indicate neural sensitivity throughout the series, and negative controls (ctrl; S-basal buffer) show no contamination across odors. Data represent 2,456 traces from 17 animals in two experiments. Odors with reduced response in odr-10 mutants are indicated by an asterisk ($P < 0.05$ via ANOVA with Benjamini–Hochberg correction). (C) Individual animal mean responses to diacetyl, S-basal buffer, and butyl acetate for WT (blue) and odr-10 mutants (red). (D and E) Peak AWA response to diacetyl is strongly correlated with a second presentation of diacetyl ($P < 0.0001$, D) but uncorrelated with response to butyl acetate ($P = 0.6$, E). Points represent mean of each animal, and error bars are SEM for three trials per animal.

behavioral response arises at a different site. Individual animals expressing GCaMP in AWA or ASH sensory neurons also showed consistent calcium transients upon diacetyl or glycerol addition, respectively, despite behavioral responses that varied across trials (Fig. 5E).

Contrasting results were obtained in the same IAA odor stimulation paradigm when calcium was monitored in the AVA command interneurons, which drive backward locomotion (29). AVA calcium levels were coupled to the behavioral output, not the sensory input, increasing during ~90% of reversals and decreasing during forward motion (Fig. 5F). The fraction responding and dynamics of the AVA response were similar to previous recordings of AVA during spontaneous reversals using high-magnification tracking systems (5–7).

Detection of Subcellular Calcium Transients in Interneurons. In AIA and AIY interneurons, calcium transients occur primarily along axonal processes rather than in cell bodies (30, 31). To accommodate weaker fluorescent signals, we used a 5×/0.25 N.A. objective and 0.63× demagnification lens for substantially higher light-gathering power at a similar spatial resolution (5.1 μm per pixel) and field of view (2.6 × 2.6 mm²) than the 2.5×/0.12 N.A. objective (Fig. 5 G and I).

We measured AIA interneuron activity in moving animals by tracking the bright cell body and integrating fluorescence in a larger region that included a portion of the axon. Calcium levels in AIA interneurons increased upon diacetyl addition and decreased immediately when odor was removed (Fig. 5H), like previously reported responses of AIA neurons to IAA odor in trapped animals (31). Calcium levels also increased in neurites of the AIY inter-

neurons upon addition of diacetyl or IAA, although no responses were observed in the AIY cell body to either odor (Fig. 5J).

Responses to Spatial Odor Patterns. Whereas temporal stimulus patterns, such as odor pulses, provide a uniform stimulus history to many animals across repeated experiments, spatial odor patterns may better approximate sensory signals experienced during goal-directed tasks such as chemotaxis. To demonstrate the ability to correlate behavior and neural activity in response to spatial chemical patterns, we used a modified microfluidic device that presented a stable ~1-mm-wide stripe of odor with a sharp interface at the stripe edge (14) (Fig. 6A and Fig. S1). As a freely moving animal left the 1-μM IAA odor stripe, AWC fluorescence increased sharply, often preceding a reversal or pirouette behavior that reoriented the animal back into the attractive odor (Fig. 6B). A second device presented a linear odor gradient (300 μM/mm IAA) across the arena (Fig. 6C). Each excursion down the odor gradient elicited AWC neural activity, frequently followed by reversal or turning behaviors that returned the animal to an elevated odor concentration (Fig. 6 D and E and Movie S4). The intervals between odor decrease, neural activation, and reversal response were longer in the shallow stimulus gradient (as much as several seconds) than they were at the sharp odor edge of a stripe; on average, an animal traversed 0.6 mm down the gradient before responding with a reorienting behavior (Fig. 6E).

Discussion

Imaging neural activity with low-magnification optics yielded substantial benefits in animal throughput, experiment duration, and repeatable chemical stimulation compared with existing
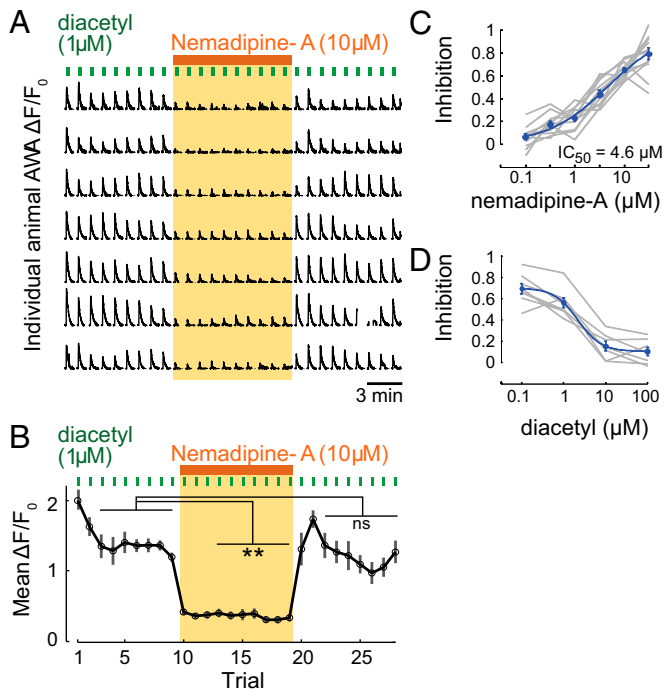
Larsch et al.

Fig. 4. Pharmacological modulation of neuronal responses to odors. (*A*) Seven animals were subjected to repeated 1-μM diacetyl odor pulses (10 s) in the presence or absence of 10 μM nemadipine-A, an L-type calcium channel antagonist. Rows represent odor-evoked AWA calcium transients in individual animals measured simultaneously. Each trial was repeated once per minute. (*B*) Peak fluorescence response per trial after odor addition. Error bars indicate SEM; $n = 7$ animals from *A* (**$P < 0.001$; ns, not significant). (*C*) Dose–response curve for nemadipine-A inhibition of responses to 1 μM diacetyl odor stimulation. Data are mean $\pm$ SEM; $n = 12$ animals, 6 trials each per concentration, one experiment. Blue curve is sigmoidal fit, and gray lines represent individual animal curves. (*D*) Dose–response curve for inhibition of diacetyl response by 10 μM nemadipine-A, which increases the EC_{50} approximately 100-fold from 30 nM (Fig. S6) to 2.5 μM DA (mean $\pm$ SEM; $n = 8$ animals, 6 trials each per concentration, one experiment).

systems for high-magnification imaging of an individual restrained or freely moving animal. We obtained wide-field recordings of activity in sensory neurons, and from interneurons whose calcium transients were restricted to their axons, despite reduced spatial resolution and fluorescent signal-to-noise ratio. For many applications, such as characterizing stochastic neural and behavioral responses, it should be beneficial to increase experimental throughput at the expense of image resolution.

Experimental reproducibility is often challenging for studies of animal behavior in which small variations in training, stimulus history, or assay conditions can substantially influence behavioral outcomes (32, 33). In our system, precisely delivered chemical stimuli elicited predictable behavior probabilities and calcium responses: population-average responses adapted consistently over time at similar rates from one experiment to another, and individuals consistently responded strongly or weakly to repeated stimuli. Whereas *C. elegans* neural recordings generally have been made in naive animals, we found that sensory calcium responses in AWA were most variable during the first few stimuli, becoming more reproducible and stable after several pulses. Defining the stable response regimes for other neurons and sensors should facilitate characterization of their properties and comparisons of their responses across experimental conditions.

The magnitude and sensitivity of odor-evoked AWA calcium dynamics varied among isogenic animals. Possible sources of this variation include developmental or epigenetic variations

between animals, effects of recent experience or modulatory state, variability associated with the GCaMP transgene, or stochastic effects. These observations emphasize the need to examine neural and behavioral responses in many individual animals under repeatable stimulation.

Continuing improvements in optical components, software, and neural sensors will likely further increase the experimental throughput of wide-field neural imaging. Cameras are already available with larger sensors for increased field of view, as are objectives with higher N.A. Improvements to analysis software, particularly for tracking many freely moving animals, will be required for full automation of data analysis.

We present here several examples of experiments enabled or accelerated by wide-field neural imaging. Mapping neural activity during probabilistic behaviors, such as decision-making in complex or conflicting sensory environments, will require large numbers of neural recordings, as will genetic and pharmacological analyses of neural response dynamics. Long-term recordings should enable the continuous study of neural and behavioral plasticity, adaptation, and learning over hours. We anticipate this reliable and efficient system will aid in the detection of subtle neural phenotypes, the study of neural dynamics, and the generation of data for systems modeling of brain circuitry.

Methods

Automated Imaging and Stimulation. We built the automated microscope on a Zeiss AxioObserver.A1 inverted body with Zeiss Fluar objective lenses (2.5×/ 0.12 N.A. or 5×/0.25 N.A.) and an Andor iXon3 DU-897 EM-CCD camera mounted with a 0.63× or 1.0× c-mount adapter. A custom-built digital timing circuit synchronized image capture with illumination pulses of adjustable duration and delay from a Lumencor SOLA-LE solid-state lamp. Metamorph 7.7.6 software controlled both image streaming (typically 10–30 frames per s for 30–60 s) and stimulus delivery via digital signals (from National Instruments NI-DAQmx to an Automate Valvebank 8 II actuator and Lee solenoid valves) and via serial commands to a Hamilton MVP eight-way distribution valve. Custom journal scripts selected from various preprogrammed recording parameters (exposure, binning, stream length, trial interval) and stimulation parameters (stimulation valve timing and odor selection valves). Fully automated experiments (tested up to 12 h) required no further user intervention after a session had been initiated.

Microfluidic Device Designs. Odor pulses were delivered by using a microfluidic device designed with a shifting-flow strategy that prevent pressure or flow rate discontinuities detectable by the animal (2) (Fig. S1*A*). One of two stimulus streams was directed into the arena by using a computer-controlled three-way valve that switched the flow position of a "control" fluid stream while the other stimulus stream bypassed the arena directly to the outflow (Fig. S1*E*).

Stripe and gradient devices were based on our previous designs (14). In the stripe device, three separate fluidic inlets provided the top, middle, and bottom fluid streams (Fig. S1*B*). In the linear gradient device, two fluid streams entered a three-stage "mixing tree" composed of converging and diverging channels that divide the flow into nine streams with linearly varying concentration (Fig. S1*C*). All spatial odor profiles were verified by using dye solutions before each experiment.

For direct comparison of neural responses in two populations (e.g., mutant vs. WT), we used a two-arena pulse device (Fig. S1*D*), modified from the standard pulse device by adding a second animal loading port and a physical barrier parallel to fluid flow. Chemical switch timing was comparable in both arenas in this design, and the chemical screen in *odr-10* mutants was performed in parallel with WT controls by using this device (Fig. 3 *B–E*).

Microfluidic Device Fabrication. We prepared monolayer microfluidic devices (Fig. S1) by using soft lithography (14). Briefly, we fabricated silicon mold masters by using conventional photolithographic techniques to pattern a 70-μm layer of SU8 2050 photoresist (Microchem) on 4-inch wafers (Silicon Quest). Photomasks were printed at 5,080 dpi (Pageworks). We cast ~5-mm-thick polydimethylsiloxane (PDMS) devices (Sylgard 184 A and B, 1:10 by weight; Dow Corning) and cored inlet and outlet holes with a 1-mm dermal punch (Accuderm). We cleaned devices in ethanol at least overnight to remove residual PDMS monomers, rinsed them in water, and baked them for
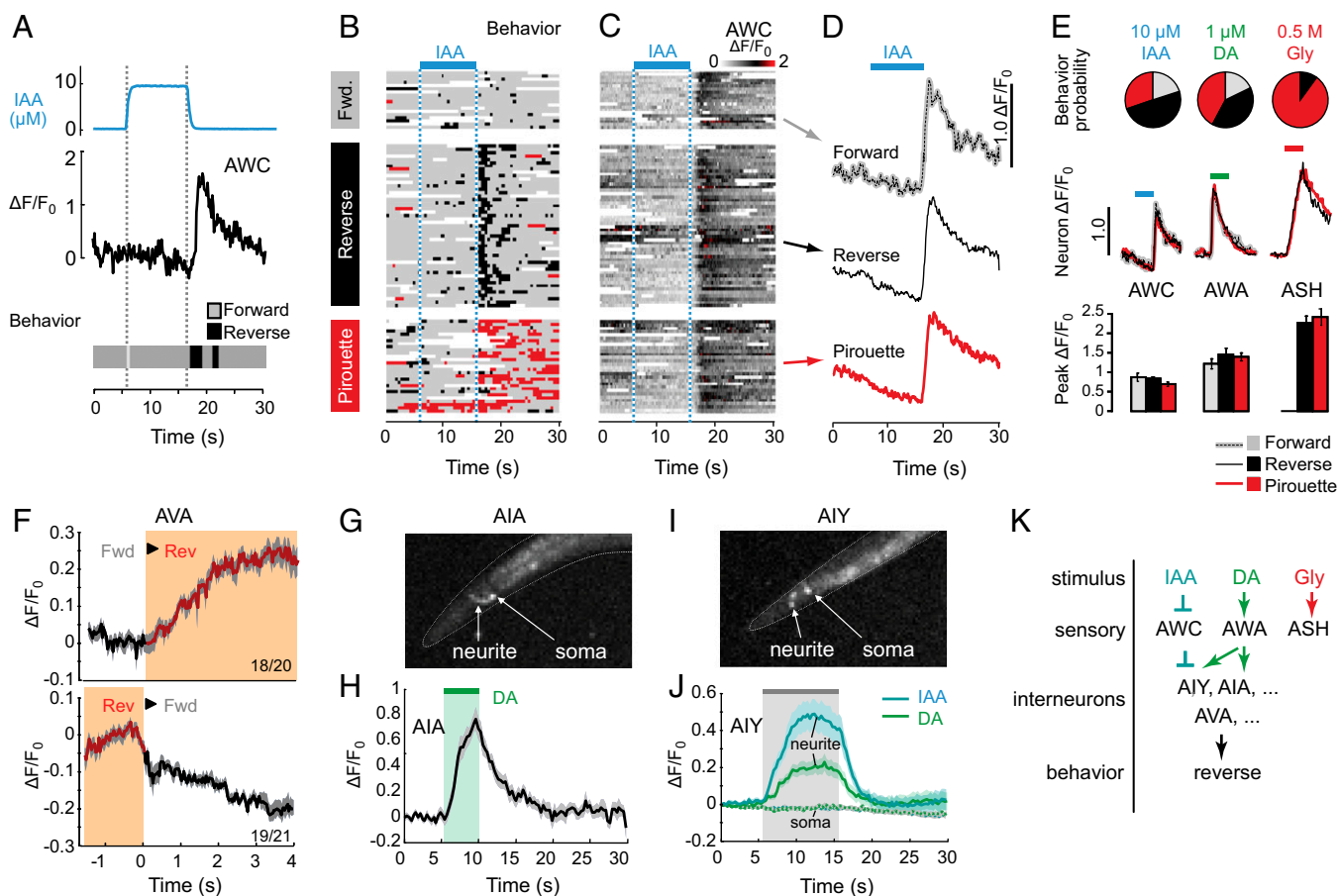
Fig. 5. Stimulus-evoked sensory neuron, interneuron, and behavioral responses. (*A*) Time course of odor stimulation, AWC[ON] neuron fluorescence, and locomotory behavior in a single animal following 10 μM IAA odor stimulation. Black indicates short reversal; gray indicates forward movement. (*B*) Ethogram of behavioral responses, grouped by predominant response to odor removal: forward (fwd.), short reverse, or pirouette (coupled reversal and Ω-turn). Red indicates the long reversal component of a pirouette response. White indicates missing data. (*C*) AWC[ON] activity corresponding to each trial (row) in *B*. (*D*) Average AWC[ON] fluorescence for each behavioral response group in *B*. (*E*) Behavior response probability and superimposed behavior–calcium average traces for AWC (data from *D*) and from AWA stimulated by 1 μM diacetyl (DA) and ASH stimulated by 0.5 M glycerol (Gly). No significant differences were seen between peak calcium levels associated with different behaviors. Data in *B–E* are from two animals tested individually per neuron–stimulus pair, 60 trials per animal. (*F*) AVA (backward command interneuron) activity in freely moving animals stimulated with IAA odor increased upon initiation of reverse movement and decreased after reversal termination. (*G*) GCaMP expression in AIA interneuron neurites and soma. (*H*) Time course of AIA response to 1 μM DA stimulation in freely moving animals. AIA fluorescence was integrated in a 6 × 6 pixel area that included the cell body and a portion of the neurite. Shading indicates SEM; *n* = 18 traces from four animals, one experiment. (*I*) AIY::GCaMP expression. The two anterior bright spots represent integrated fluorescence across the neurite. (*J*) AIY responses to 10-s pulses of 10 μM IAA and 1 μM DA recorded at the neurite or soma in stationary animals. Shading indicates SEM; *n* = 70 traces from seven animals, one experiment. (*K*) Partial list of neurons transducing stimulus information to behavioral response. Pointed and T-shaped arrows indicate functional excitatory and inhibitory interactions confirmed in this work, respectively.

at least 30 min at 55 °C to evaporate any absorbed ethanol. Devices were reversibly sealed against a hydrophobic 25 × 50 mm glass slide, prepared by exposure to (tridecafluoro-1,1,2,2-tetrahydrooctyl)-1-trichlorosilane (United Chemical Technologies) vapor for 1 h under vacuum. We placed a support glass slide containing inlet and outlet holes drilled with a diamond-coated bit above the PDMS device and clamped it in a stage adapter (P-2; Warner Instruments) modified with longer screws and rubber washers.

We regulated flow velocities in the arena from 0.1 to 2 mm·s⁻¹ by gravity proportional to the height differential between stimulus and outflow reservoir surfaces, from 5 to 150 cm. Fluidic connections were made with microbore tubing (Tygon S-54-HL; 0.020-inch ID) containing a metal tube (NE-1027-12; New England Small Tubing) on one end for insertion into the microfluidic device and a Luer stub needle on the other for connection to a valve, reservoir, or syringe. We used high-purity Teflon perfluoroalkoxy tubing (IDEX) to prevent cross-contamination when presenting multiple stimuli within an experiment. Stimuli were delivered from 30-mL syringe reservoirs (Fig. S1*F*). Alternatively, as many as eight stimuli were directed through an electrically actuated distribution valve, e.g., for a dose–response curve (Fig. S1*G*). For chemical screening, stimulus streams were fed from a 96-well plate (Fig. S1*H*).

Strains. *C. elegans* were maintained under standard conditions and fed OP50 bacteria (34). WT worms were Bristol strain (N2). The following strains expressed GCaMP variants in different neurons:

AWA: CX14887, *kyIs598* [*gpa-6::GCaMP2.2b* 50 ng/μL]

AWA *odr-10*: CX15127, *odr-10(ky32)*; *kyIs598*

AWC: CX14215, *kyEx4467* [*str-2::GCaMP5 D380Y* 50 ng/μL]

ASH: CX10979, *kyEx2865* [*sra-6::GCaMP3* 100 ng/μL]

AVA: CX15380, *kyEx5170* [*rig-3::GCaMP5.0* 30 ng/μL]

AIA: CX14034, *kyEx4345* [*gcy-28d::GCaMP2.2b* 50 ng/μL]

AIY: CX14780, *lite-1(ce314)*; *kyEx4857* [*mod-1::GCaMP5* 25 ng/μL]

The GCaMP cDNAs were provided by Loren Looger (Janelia Farm Research Campus, Howard Hughes Medical Institute, Ashburn, VA) and subcloned into the pSM vector using NotI restriction sites. Neuron-selective promoters were exchanged using FseI and AscI sites flanking the promoter sequence in this vector. Transgenic animals were generated by injecting DNA clones and a fluorescent coinjection marker (*ofm-1:: dsRED*) into gonads of young adult hermaphrodites. We performed
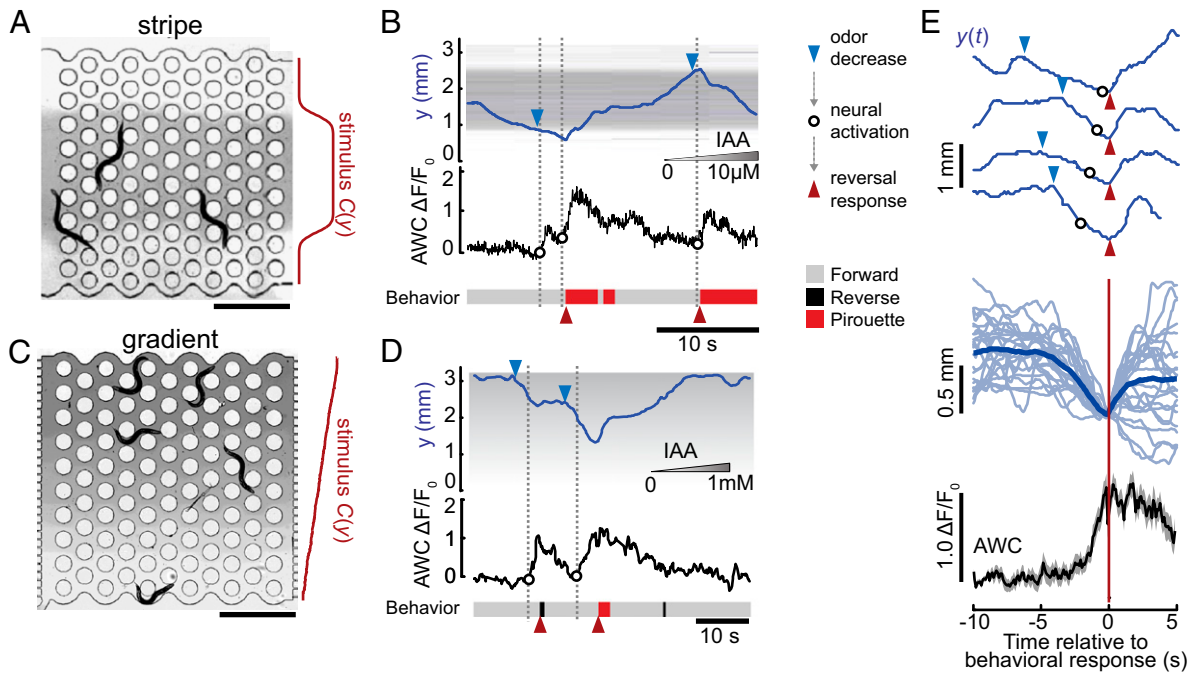
Larsch et al.

www.manaraa.com

Fig. 6. Neural and behavioral responses of freely moving animals in spatial odor patterns. (*A*) Bright-field image of the microfluidic arena presenting a stable horizontal fluidic stripe (visualized with dye). (Scale bar, 1 mm.) (*B*) Time course of *y* axis position and AWC neuron fluorescence of a single animal responding to a stripe of IAA odor. Vertical lines and open circles indicate the onset of AWC activity increase, which coincided with odor decrease at the lower or upper stripe edge (blue arrowheads) and preceded the onset of behavioral responses (red arrowheads). (*C*) Bright-field image of a linear odor gradient (visualized with dye). (Scale bar, 1 mm.) (*D*) *y* Axis position and AWC fluorescence of one animal responding to a linear IAA gradient. Labels are as in *B*. (*E*) Temporal alignment of position in a linear gradient to the initiation of reversal or pirouette responses. Four representative descents are shown, indicating the onset of gradient descent (blue arrowheads), increased AWC activity (circles), and behavioral response (red arrowheads). (*Lower*) Individual trajectories, mean relative position, and mean AWC fluorescence for 24 gradient descents aligned to the onset of reversal response. Shading indicates SEM; *n* = 2 animals from independent experiments.

multicopy integration of the *gpa-6::GCaMP2.2b* extrachromosomal array using UV irradiation, and the resulting strain CX14887 was back-crossed six times to WT *C. elegans*.

To provide age-synchronized young adults for each experiment, we picked L4 larval-stage animals onto agar plates 15 to 20 h earlier. Immediately before each experiment, we gently transferred 1 to 25 worms onto a fresh, unseeded agar plate with a small amount of bacteria. After removing excess bacteria, we flooded the plate with ~5 mL S-basal buffer (100 mM NaCl and 50 mM potassium phosphate, pH 6.0). Swimming animals were then drawn into worm-loading tubing by using a 1-mL syringe.

Stimulus Preparation. Odor dilutions were prepared fresh on the day of the experiment from pure stock solutions (IAA, diacetyl, glycerol) or from 1:100 dilutions in ethanol for odor screening. Dilutions were made in S-basal buffer. Where mentioned, 1 mM (-)-tetramisole hydrochloride (Sigma) was added to S-basal buffer to paralyze body wall muscles and keep animals stationary.

Experimental Setup. We assembled the microfluidic arenas and degassed them in a vacuum desiccator for at least 10 min before loading S-basal buffer through the outlet port. This step ensures that any air bubbles absorb quickly into the PDMS. We connected tubing from the stimulus and control reservoirs to the arena and flushed the device with S-basal buffer. Next, we attached the loading tubing and gently injected 1 to 25 worms via syringe into the arena. Typically, 10 to 20 animals were loaded when animals were paralyzed during imaging, and one or two animals were loaded for freely moving animals, to facilitate tracking. Buffer flow continuously washed the animals, removing any residual bacteria. Experiments in freely moving worms began typically after 15 to 20 min in the device and 30 min after removal from bacterial food, when local search behaviors had subsided. For experiments in tetramisole-paralyzed worms, we allowed 60 min of buffer flow for maximal paralysis. For repeated stimulation, we preconditioned animals with 5 to 10 trials to stabilize responses, except for the dose–response experiment in Fig. 2, in which we report responses of naive animals.

After each experiment, we flushed arenas with water and soaked them in ethanol for 24 h to remove any residual odor. Next, we rinsed devices in water, dried them in an air stream, and baked them at 55 °C for at least 30 min. After this cleaning procedure, buffer–buffer controls showed no response, and devices could be reused more than 30 times.

Data Analysis and Statistics. We analyzed movies for neural fluorescence and locomotory behavior by using the NeuroTracker software suite, a set of custom ImageJ macros and MATLAB scripts described in *SI Note*. Typically, 70% to 90% of animals in the device could be tracked. Background-corrected integrated neural fluorescence traces $F(t)$ were divided by baseline fluorescence F_0 (mean for the first 5 s) to obtain the normalized calcium response ($\Delta F/F_0$) for each animal and stimulation trial. Normalized traces were then averaged across repeated trials for each animal. Population-average responses report the mean and variance of individual animal responses. Statistical comparisons were made by ANOVA using Bonferroni correction for multiple comparisons, or the Benjamini–Hochberg correction where indicated. Data are presented from one experiment unless otherwise stated.

Neuronal calcium response dynamics were quantified as the peak fluorescence and peak delay time determined for each animal and trial from normalized fluorescence traces smoothed with a 0.3-s window. Unless otherwise stated, we averaged calculated response parameters from repeated trials for each animal and reported statistics on the variance between animals. Peak fluorescence was calculated as maximum fluorescence during the stimulus pulse (stim) minus maximum fluorescence during the 2-s (20 frames) period before stimulation (prestim): $\max(\Delta F/F_0)_{stim} - \max(\Delta F/F_0)_{prestim}$. Peak delay time was determined as the time after stimulus onset when maximum fluorescence occurred.

Variance across repeated trials and across animals (Fig. 2*D*) was calculated by using the MATLAB "var" function on peak calcium fluorescence per neural trace. Dose–response curves were fit using the MATLAB curve-fitting toolbox and function "cfit" to a four-parameter sigmoidal curve defined by $F' = F'_{min} + (F'_{max} - F'_{min})/[1 + (EC_{50}/C)^{\beta}]$, where $F' = \Delta F/F_0$ for each trace and C is odor concentration. EC_{50} represents the odor concentration eliciting a 50% maximal peak response and the parameter β represents the dynamic range of the response.

www.manaraa.com

Gradient Quantification. For experiments involving changes in the stimulus gradient dC/dt (Fig. 2 *G* and *J*), we measured dC/dt and stimulus timing in the imaging arena at different flow rates in separate dye experiments. dC/dt in the imaging arena was calculated by imaging fluorescein dye switched against buffer. We used the Matlab function "polyfit" to calculate the slope of increase in normalized dye fluorescence during four frames surrounding half maximal fluorescence.

1. Faumont S, Lockery SR (2006) The awake behaving worm: Simultaneous imaging of neuronal activity and behavior in intact animals at millimeter scale. *J Neurophysiol* 95(3):1976–1981.
2. Chronis N, Zimmer M, Bargmann CI (2007) Microfluidics for in vivo imaging of neuronal and behavioral activity in *Caenorhabditis elegans*. *Nat Methods* 4(9):727–731.
3. McCormick KE, Gaertner BE, Sottile M, Phillips PC, Lockery SR (2011) Microfluidic devices for analysis of spatial orientation behaviors in semi-restrained *Caenorhabditis elegans*. *PLoS ONE* 6(10):e25710.
4. Wen Q, et al. (2012) Proprioceptive coupling within motor neurons drives *C. elegans* forward locomotion. *Neuron* 76(4):750–761.
5. Ben Arous J, Tanizawa Y, Rabinowitch I, Chatenay D, Schafer WR (2010) Automated imaging of neuronal activity in freely behaving *Caenorhabditis elegans*. *J Neurosci Methods* 187(2):229–234.
6. Faumont S, et al. (2011) An image-free opto-mechanical system for creating virtual environments and imaging neuronal activity in freely moving *Caenorhabditis elegans*. *PLoS ONE* 6(9):e24666.
7. Piggott BJ, Liu J, Feng Z, Wescott SA, Xu XZS (2011) The neural circuits and synaptic mechanisms underlying motor initiation in *C. elegans*. *Cell* 147(4):922–933.
8. Zheng M, Cao P, Yang J, Xu XZS, Feng Z (2012) Calcium imaging of multiple neurons in freely behaving *C. elegans*. *J Neurosci Methods* 206(1):78–82.
9. Wilson MA, McNaughton BL (1993) Dynamics of the hippocampal ensemble code for space. *Science* 261(5124):1055–1058.
10. Dombeck DA, Khabbaz AN, Collman F, Adelman TL, Tank DW (2007) Imaging large-scale neural activity with cellular resolution in awake, mobile mice. *Neuron* 56(1):43–57.
11. Maimon G, Straw AD, Dickinson MH (2010) Active flight increases the gain of visual motion processing in *Drosophila*. *Nat Neurosci* 13(3):393–399.
12. Ghosh KK, et al. (2011) Miniaturized integration of a fluorescence microscope. *Nat Methods* 8(10):871–878.
13. Ahrens MB, et al. (2012) Brain-wide neuronal dynamics during motor adaptation in zebrafish. *Nature* 485(7399):471–477.
14. Albrecht DR, Bargmann CI (2011) High-content behavioral analysis of *Caenorhabditis elegans* in precise spatiotemporal chemical environments. *Nat Methods* 8(7):599–605.
15. Clokey GV, Jacobson LA (1986) The autofluorescent "lipofuscin granules" in the intestinal cells of *Caenorhabditis elegans* are secondary lysosomes. *Mech Ageing Dev* 35(1):79–94.
16. Coburn C, et al. (2013) Anthranilate fluorescence marks a calcium-propagated necrotic wave that promotes organismal death in *C. elegans*. *PLoS Biol* 11(7):e1001613.
17. Bargmann CI, Hartwieg E, Horvitz HR (1993) Odorant-selective genes and neurons mediate olfaction in *C. elegans*. *Cell* 74(3):515–527.
18. Shinkai Y, et al. (2011) Behavioral choice between conflicting alternatives is regulated by a receptor guanylyl cyclase, GCY-28, and a receptor tyrosine kinase, SCD-2, in AIA interneurons of *Caenorhabditis elegans*. *J Neurosci* 31(8):3007–3015.
19. Lewis JA, Wu CH, Levine JH, Berg H (1980) Levamisole-resistant mutants of the nematode *Caenorhabditis elegans* appear to lack pharmacological acetylcholine receptors. *Neuroscience* 5(6):967–989.
20. Bargmann CI (2006) Chemosensation in *C. elegans* (October 25, 2006). *WormBook*, ed. The *C. elegans* Research Community, WormBook, doi/10.1895/wormbook.1.123.1, http://www.wormbook.org.
21. Sengupta P, Chou JH, Bargmann CI (1996) *odr-10* encodes a seven transmembrane domain olfactory receptor required for responses to the odorant diacetyl. *Cell* 84(6):899–909.
22. Petrascheck M, Ye X, Buck LB (2007) An antidepressant that extends lifespan in adult *Caenorhabditis elegans*. *Nature* 450(7169):553–556.
23. Kwok TCY, et al. (2006) A small-molecule screen in *C. elegans* yields a new calcium channel antagonist. *Nature* 441(7089):91–95.
24. Lockery SR, et al. (2012) A microfluidic device for whole-animal drug screening using electrophysiological measures in the nematode *C. elegans*. *Lab Chip* 12(12):2211–2220.
25. Suzuki H, et al. (2003) *In vivo* imaging of *C. elegans* mechanosensory neurons demonstrates a specific role for the MEC-4 channel in the process of gentle touch sensation. *Neuron* 39(6):1005–1017.
26. Hilliard MA, et al. (2005) *In vivo* imaging of *C. elegans* ASH neurons: Cellular response and adaptation to chemical repellents. *EMBO J* 24(1):63–72.
27. Busch KE, et al. (2012) Tonic signaling from O₂ sensors sets neural circuit activity and behavioral state. *Nat Neurosci* 15(4):581–591.
28. Pierce-Shimomura JT, Morse TM, Lockery SR (1999) The fundamental role of pirouettes in *Caenorhabditis elegans* chemotaxis. *J Neurosci* 19(21):9557–9569.
29. Chalfie M, et al. (1985) The neural circuit for touch sensitivity in *Caenorhabditis elegans*. *J Neurosci* 5(4):956–964.
30. Chalasani SH, et al. (2007) Dissecting a circuit for olfactory behaviour in *Caenorhabditis elegans*. *Nature* 450(7166):63–70.
31. Chalasani SH, et al. (2010) Neuropeptide feedback modifies odor-evoked dynamics in *Caenorhabditis elegans* olfactory neurons. *Nat Neurosci* 13(5):615–621.
32. Wahlsten D, et al. (2003) Different data from different labs: Lessons from studies of gene-environment interaction. *J Neurobiol* 54(1):283–311.
33. Richter SH, Garner JP, Würbel H (2009) Environmental standardization: Cure or cause of poor reproducibility in animal experiments? *Nat Methods* 6(4):257–261.
34. Brenner S (1974) The genetics of *Caenorhabditis elegans*. *Genetics* 77(1):71–94.

Larsch et al.

www.manaraa.com